Sigma J Eng & Nat Sci 36 (4), 2018, 1009-1022

Sigma Journal of Engineering and Natural Sciences
Sigma Mühendislik ve Fen Bilimleri Dergisi

Research Article

NONLINEAR SEISMIC BEHAVIOR OF A HISTORICAL DAM FOR DIFFERENT SOIL GROUPS

Musa YETKİN*[1], Yusuf CALAYIR[2], Erkut SAYIN[3], Muhammet KARATON[4]

[1]*Fırat University, Civil Engineering Department, ELAZIG;* ORCID: 0000-0002-6259-4137
[2]*Fırat University, Civil Engineering Department, ELAZIG;* ORCID: 0000-0002-6387-5360
[3]*Fırat University, Civil Engineering Department, ELAZIG;* ORCID: 0000-0003-0266-759X
[4]*Fırat University, Civil Engineering Department, ELAZIG;* ORCID: 0000-0002-1498-4659

Received: 09.05.2018 Accepted: 25.07.2018

ABSTRACT

In this study, effect of soil flexibility on non-linear seismic response of historical Sultan Mahmut dam which is constructed as masonry arch dam type is investigated. Crest displacement and damage of the dam are evaluated. Smeared crack model which includes the strain softening is used in the nonlinear analysis for the behavior of dam material. Reservoir and soil domains are assumed to be linear elastic. Solid-fluid interaction is considered by Eulerian approach. For seismic input, artificial acceleration records are generated for four different soil groups (A, B, C and D) considering D2 seismic level. These records are acted in the stream direction to the dam-soil-reservoir system. Effect of soil flexibility on seismic response of the dam is evaluated for each soil group. ANSYS finite element program is used for the solutions.
Keywords: Solid-fluid interaction, smeared crack model, artificial acceleration records, nonlinear seismic analysis.

1. INTRODUCTION

Historical dams are cultural heritage that must be preserved. Dams are usually built to provide irrigation or drinking water. In addition to their own weight loads, they are also exposed to additional loads due to dam-soil and dam-fluid interactions. Depending on the earthquake effect, there are usually significant increases in the mentioned interaction loads. There is a need to know seismic performances of historical structures and to take necessary measures to minimize the damage and to preserve their structural integrity during an earthquake. In the numerical modeling of masonry constructions, three different modeling techniques are used, micro, meso (simplified micro) and macro modeling, based on the size of the building system. Large-scale masonry building systems are often modeled using macro modeling techniques [1]. Betti and Vignoli [2] investigated the structural behavior and seismic damage possibility of a Roman-style masonry church, the Farneta, by creating a mathematical model using macro-modeling. Riva et al. [3] conducted a seismic analysis by modeling the Asinelli tower in Italy using the macro modeling technique. Fanning and Boothby [4] modeled three masonry bridges using macro modeling

* Corresponding Author: e-mail: musayetkin@firat.edu.tr, tel: (424) 237 00 00 / 5426

methods and investigated these bridges under static loads in their study. In that study, a smeared fracture model was used for structural elements. Bernardeschi et al. [5] modeled Buti bell tower in Italy with macro modeling technique under two different conditions of under its own weight and its own weight and a horizontal load effect. Bayraktar et al. [6] constituted a finite elements model of the Haghia Sofia Bell To wer in Trabzon using the macro-modelling method, and they conducted a non-linear dynamic analysis of the tower. Mridha and Maity [7] investigated nonlinear response of concrete gravity dam-reservoir system by conducting experiments on small scale model of Koyna dam. The experimental results are compared with the analysis results due to tensile damage. Soumya et al. [8] used time history analysis to analysis the probable failure patterns of a dam about 120 years old. They carried out an analysis to estimate stress in the dam for three histories with different PGA values. Sayın [9] evaluated seismic response of a masonry bridge using artificial acceleration records considering the seismic characteristics of the region where the bridge was located. Sayın et al. [10] investigated nonlinear analysis of historical Topuzlu Dam under various seismic loads taking into account the solid-fluid interaction. Karaton et al. [11] conducted nonlinear seismic response of a 12th century historical masonry bridge under three different earthquake levels. Zacchei et al. [12] described seismic hazard performance on the site of Rules Dam, in Granada province in Spain. Yazdani and Alembagheri [13] investigated nonlinear seismic response of a gravity dam under near-fault ground motions. For this purpose, Pine Flat dam was considered. It was numerically modelled using the finite element method base on Eulerian-Lagrangian approach. Wang et al. [14] evaluated investigation of the seismic cracking behavior of Guandi concrete gravity dam, which is located in China. For this purpose, three dimensional nonlinear finite element analyses of the Guandi dam-reservoir-foundation system were carried out. Obtained results showed that the significant influence of contraction joints and cross-stream ground motions on the dynamic response and damage-cracking risk of the Guandi concrete gravity dam.

In this study, nonlinear dynamic analyses were performed for historical masonry Sultan Mahmut Dam, using design acceleration spectrum compliant artificial earthquake acceleration records based on D2 level earthquake effect for four different soil groups. The effect of the soil elasticity on the seismic behavior of the dam was evaluated. In the nonlinear analysis, a smeared crack model that takes strain softening into account was used for dam material. It was accepted that reservoir and soil domains demonstrated linear behavior. The solid-fluid interaction was considered with the Euler approach. For dynamic analysis, the combined form of the generalized α algorithm with prediction-correction method was used [15].

2. HISTORICAL SULTAN MAHMUT DAM

Sultan Mahmut dam is one of the dam of Taksim facilities in Istanbul and is located on the west branch of the Arabacı Mandırası stream at Bahçeköy which is one of the branches of Kâğıthane stream. It was built by Mahmut II and completed in 1839. The time of construction is the last of the three dams of Taksim facilities. This bend, also called Bend-i Cedit (New Dam), had been constructed as masonry belt dam. The top of Sultan Mahmut Dam is inclined towards the downstream side and covered with marble plaques (Figure 1). The dam hydrological region is 830000 m^2, crest height is 15.45 m, crest length is 101.55 m and reservoir volume is 343325 m^3 [16].

Figure 1. Sultan Mahmut Dam

3. NUMERICAL MODELING OF MASONRY STRUCTURES

The three techniques displayed in Figure 2 are commonly used in the modeling of masonry structures [17]. These are detailed micro modeling, simplified micro modeling, and macro modeling. In detailed micro modeling, the masonry unit and material properties of the material, namely the elasticity modulus, Poisson ratio and unit volume weights are evaluated separately. Although this is a precise modeling technique, the time required for the analysis of the complete structure takes very long. Thus, it is useful for the analysis of small buildings or parts of large structures.

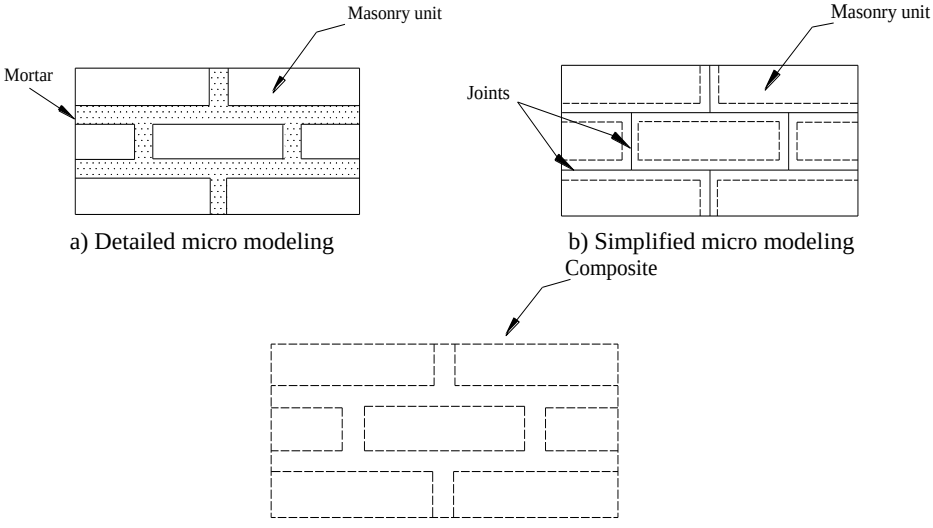

a) Detailed micro modeling

b) Simplified micro modeling

c) Macro modeling

Figure 2. Modeling techniques for masonry structures

In simplified micro modeling, the mortar layer is neglected by expanding the sizes of the masonry units to half the thickness of the mortar layer. The masonry units are separated from each other by the interface lines. It is accepted that the cracks that would form in the system will take place on these interface lines.

In macro modeling, an equivalent composite material model is selected without distinguishing between masonry units such as stone, brick, etc. and mortar. In modeling of large systems, macro modelling are often preferred because it significantly reduce the time of analysis. In this study, the masonry dam was modeled using the macro modeling technique.

Fracture and damage mechanics methods could be used for nonlinear analysis of structures for which a mathematical model was constructed with macro modeling technique. Today, cracks in fracture mechanics are investigated using two different crack models; global (discrete crack) and local (smeared crack and damage mechanics) approaches. In the discrete crack approach, cracks are modeled by defining a discontinuous region in a continuous medium. In the smeared crack approach, the constitutive equations which represent the behavior of the material are used by changing these equations based on the level and the state of the crack.

Damage mechanics is a local approach and based on the same philosophy as the smeared crack model [18, 19].

3.1. Smeared crack model

In this study, a three-parameter concrete model, which is a special condition of the William and Warnke (1975) model, was used for the smeared crack model [20]. The three parameter model was developed by William and describes the collapse surface for concrete in sections subjected to tension under low pressure. Zeinkiewicz and Taylor [21] stated that this material model could be used for material with brittle properties, such as concrete. William Warnke's concrete collapse surface model could be used effectively in the global modeling of masonry structures [4, 22]. This model, as shown in Figure 3.a, has a cone-like view with a convex cross section. Convex cross section has a symmetrical and smooth. In this Figure, σ_{xp}, σ_{yp} and σ_{zp} show principal stresses perpendicular to each other, and fc is the uniaxial compressive strength of the material. Since such a cross section could easily be transformed into a circle, von Mises and Drucker-Prager approaches could be obtained as special cases of this model [21, 23]. In this model, when the tensile values within limits of the collapse surface are obtained, it is accepted that the material exhibits linear elastic behavior and cracking and crushing would occur in the material at tensile values outside the collapse surface. It is accepted that crack usually occurs at the integration points on the element in the finite element applications with smeared crack approach.

The existence of a crack at an integration point is indicated by the rearrangement of the matrix connecting the stress to the strain by defining a weak plane in the normal direction to the crack. This arrangement is obtained as a result of the variation in the elasticity modulus. The aforementioned variation could be observed on the uniaxial tensile stress-strain relationship given in Figure 3.b. In this figure, f_t shows the uniaxial tensile strength of the material, T_c is the tensile strength reduction coefficient immediately after cracking, E is the initial elasticity modulus, and R_t is the elasticity modulus calculated in the crack softening zone. In addition, ε_{ck} and $6\varepsilon_{ck}$ shows the cracking threshold strain and ultimate strain, respectively.

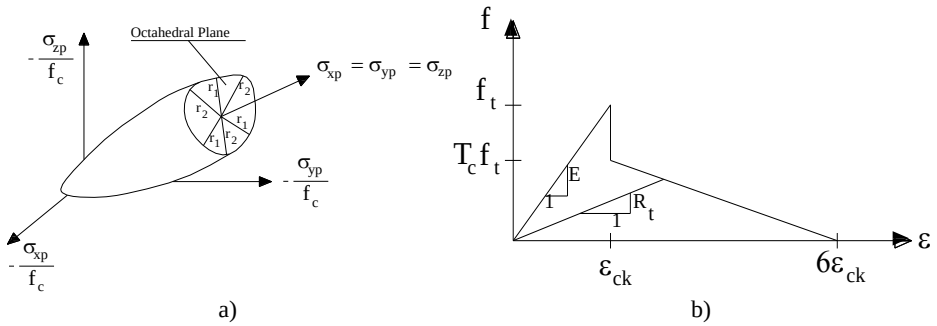

Figure 3. Three parameter concrete model a) yield surface and b) uniaxial stress-strain relationship

4. NUMERICAL APPLICATION

In this study, the effect of soil flexibility on the nonlinear seismic behavior of the historical Sultan Mahmut dam is examined. For the behavior of dam material, smeared crack model which includes the strain softening is used in the nonlinear analysis. It was accepted that both reservoir and soil domains demonstrated linear behavior. The solid-fluid interaction was taken into account with the Eulerian approach. The finite element mesh for the dam-soil-reservoir system is presented in Figure 4. A nodal point which is located in the crest of the dam was also presented on this mesh. 4224, 12996 and 7380 rectangular prismatic elements were used for the dam, soil and fluid domains, respectively. 27867 node points was used in the finite element mesh of the dam-soil-reservoir system.

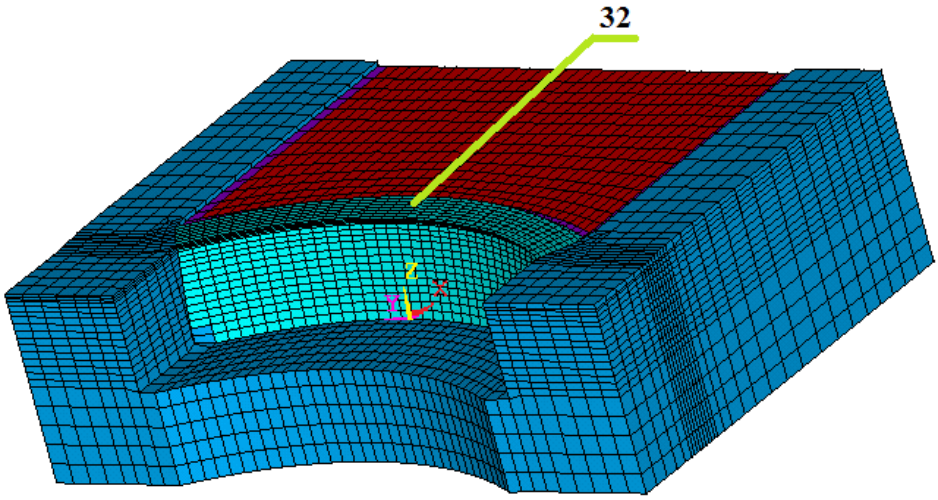

Figure 4. Three-dimensional finite element model of dam-soil-reservoir system

For the seismic effect, artificial earthquake acceleration records were generated in accordance with the design acceleration spectrum (DLH-2007) provided in the Earthquake Technical Regulation for Coastal and Harbor Structure, Railway, and Airports Constructions [24]. These acceleration records were obtained by considering four different soil groups (groups A, B, C and

D) for the D2 earthquake level. The D2 level represents large earthquakes that do not have a strong possibility of occurrence during service life of structures. The probability of exceeding this earthquake level within 50 years is 10% and its return period is 475 years. These acceleration records were applied in the flow (-x) direction to the dam-soil-reservoir system for each soil class. However, according to DLH-2007, it is necessary to point out that at least three artificial acceleration records should be used for design purposes. Reference S_{MS} and S_{M1} values (DLH-2007) used for the production of artificial acceleration records for selected soil groups are given in Table 1. Artificial acceleration records were generated so that the mean difference between the artificial and reference acceleration spectra would not exceed 5%. Artificial and reference acceleration spectrum curves for A, B, C and D soil groups are presented in Figure 5.

The absolute maximum amplitudes of the artificial earthquake records were 0,2660g, 0,3654g, 0,3510g and 0,3890g for the soil groups A, B, C and D, respectively (Figure 6). For the dynamic analysis, the combined form of the generalized α algorithm with the predict-correct method was used. Solutions were obtained with the ANSYS finite element software.

Table 1. Reference S_{MS} ve S_{M1} values for selected soil groups

	A Group	B Group	C Group	D Group
S_{MS}	0,5520	0,6900	0,7756	0,8611
S_{M1}	0,2800	0,3500	0,5075	0,5950

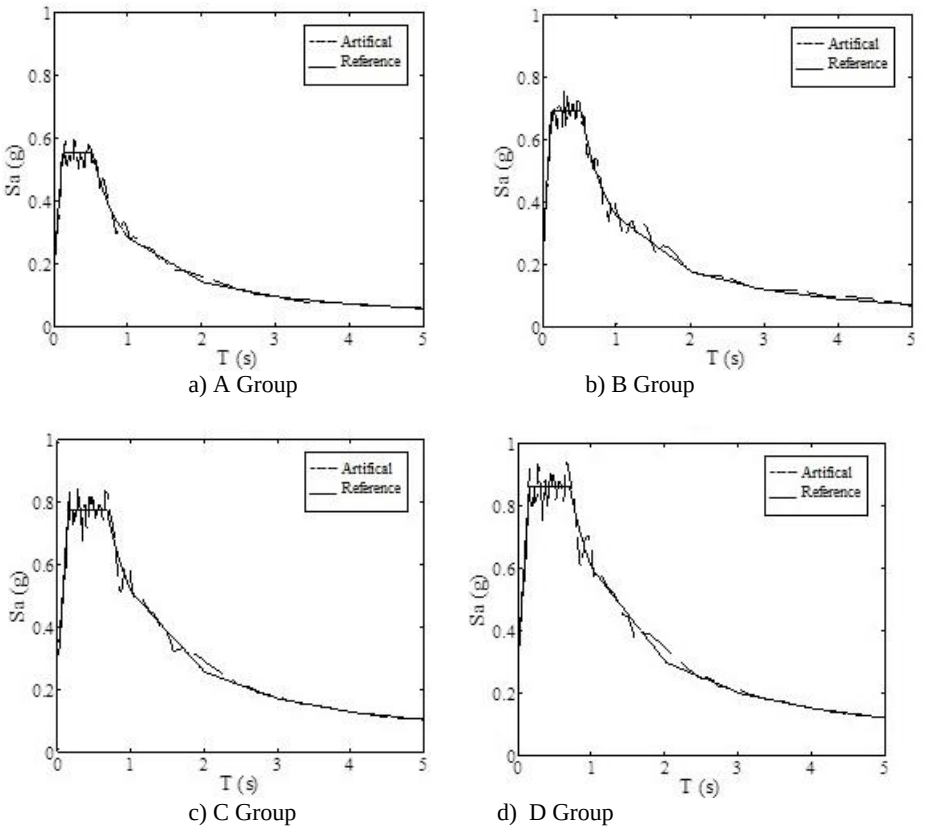

a) A Group b) B Group

c) C Group d) D Group

Figure 5. Artificial and reference acceleration spectrum curves for A, B, C and D soil groups

The elasticity modulus for the dam material was selected as 7500 MPa, the unit volume mass as 2200 kg/m^3, the Poisson ratio as 0,25, the compressive strength as 10 MPa and the tensile strength as 1,0 MPa. The tensile strength reduction coefficient immediately after the crack was selected as 1. The soil was considered massless and the material properties of selected soil groups are given in Table 2. In the table, E_b and E_t indicate the elasticity modulus for the soil and the dam, respectively, and υ shows Poisson ratio of the soil. As the soil group changes from A to D, the elasticity modulus decreases, in other words, the soil softens. The mass density and the bulk modulus of the fluid in the reservoir was accepted as 1000 kg/m^3 and 2070 MPa, respectively.

Damping proportional stiffness was taken into account for the solid domain. The base frequencies in the flow direction of the dam-soil system were 12,0445 Hz, 10,4324 Hz, 7,73659 Hz and 4,95437 Hz for the soil groups A, B, C and D, respectively. The stiffness-proportional damping coefficient for the dam- soil system was calculated so that a damping ratio of 5% is obtained at the base frequency for each soil group. The integration time step was assumed to be 0,01 s, which is the earthquake recording interval, in the linear behavior, while 0,001 s was assumed in the nonlinear behavior. In addition, the maximum number of iterations in the nonlinear behavior was assumed as 40.

Table 2. Material properties of selected soil groups

Soil Group	E_b / E_t	E_t (kN/m^2)	υ
A	0,25	30000000	0,20
B	1	7500000	0,25
C	4	1875000	0,30
D	16	468750	0,35

Nonlinear seismic solutions for the dam-soil-reservoir system were obtained using artificial earthquake acceleration records generated for different soil groups. Time history displacement of the nodal point 32 located in the central region of the crest in the flow direction is shown in Figure 7 for the soil groups A, B, C and D.

In the soil group A, the analysis continued for 11 s, which was the earthquake recording period, the dam exhibited elastic behavior and no damage occurred in the dam. However, the maximum number of iterations in the analyses was exceeded and the analyses were terminated by the software before the earthquake recording period was completed due to the damages in the dam in other three soil groups. In the displacement-time graphs (Figure 7.b, c, d) where the dam damage occurs, the numbers on the figures depict the moments when the dam damage status was identified.

Maximum and minimum displacements in the dam crest are presented in Table 3 for four different soil groups. As could be observed in the table, the displacement increased as the soil softened.

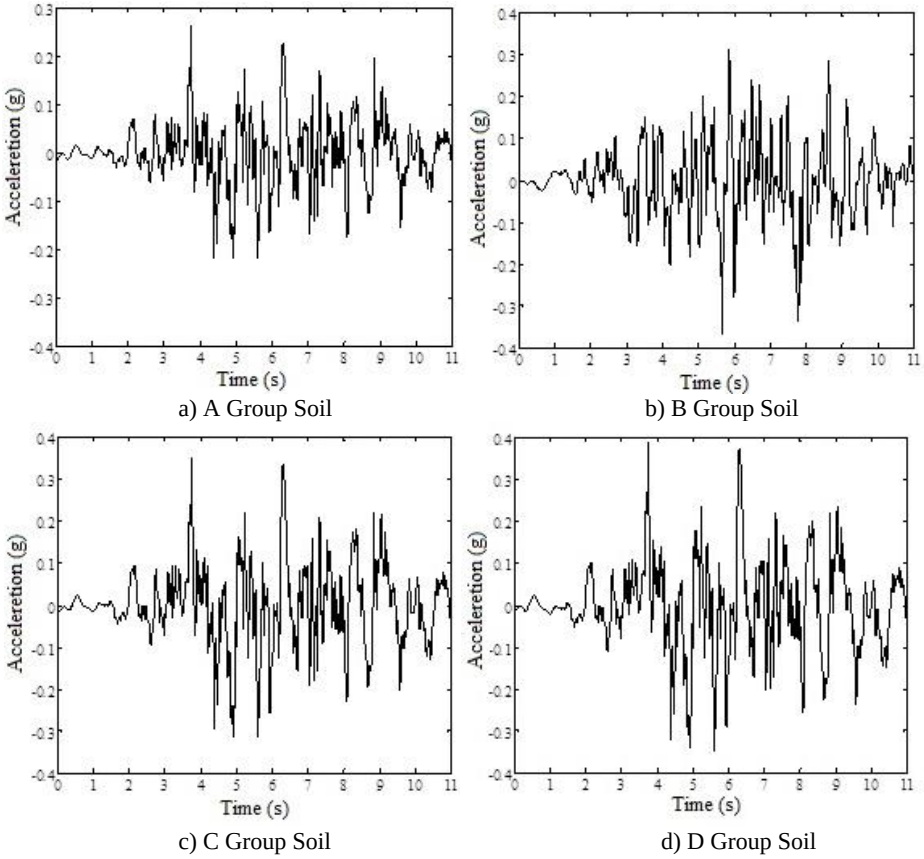

a) A Group Soil b) B Group Soil

c) C Group Soil d) D Group Soil

Figure 6. Artificial earthquake acceleration records generated for A, B, C and D soil groups

Table 3. Maximum and minimum displacements in the dam crest

	Soil Group			
	A	B	C	D
Maximum displacement (mm)	2,296	3,431	5,023	10,59
Minimum displacement (mm)	-1,997	-3,374	-4,511	-14,55

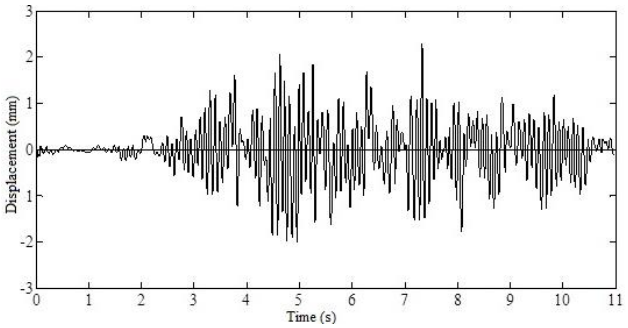

a) A Group Soil

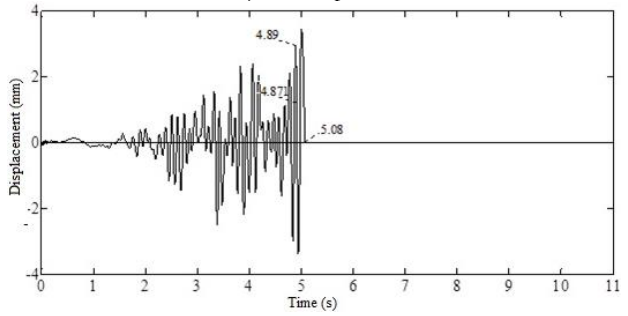

b) B Group Soil

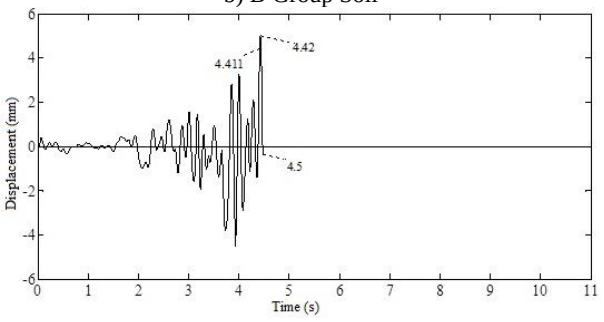

c) C Group Soil

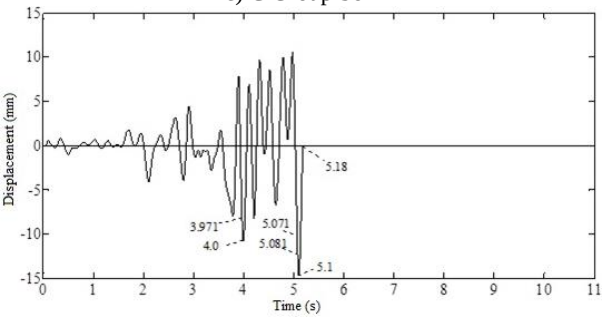

d) D Group Soil

Figure 7. Time history displacement of the dam crest in the flow direction for the soil groups A, B, C and D

It was accepted that damage to the dam (cracking or crushing) occurred at element integration points. The crack that occurred at an element integration point was represented by a hollow circle when open, and by the symbol when closed. As mentioned above, there was no damage to the dam in group A soil. For group B soil, the first damage occurred at 4,871 s at the mid-section of dam-soil interface where the tensile stress reached high values as the dam crest was moving towards the flow direction (Figure 8.a). Until 4,89 s, when the movement of the dam crest continued in the flow direction, the corresponding crack area expanded slightly towards both slopes (Figure 8.b). At 5,08 s, when the analysis was terminated due to the damage, the existing crack area increased significantly both in the direction of the slopes and in the flow direction (Figure 8.c).

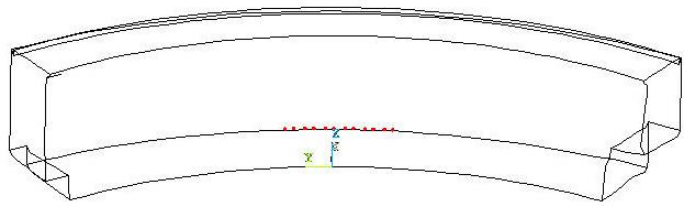

a) t=4,871 s

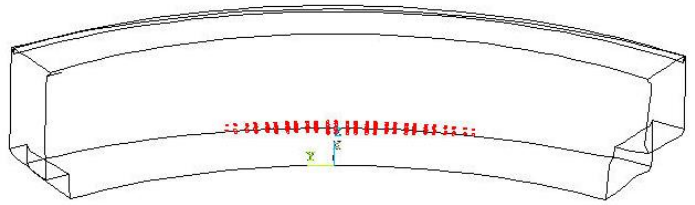

b) t=4,89 s

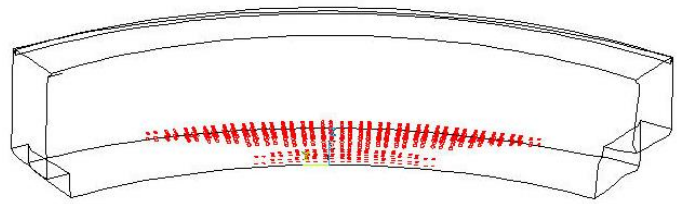

c) t=5,08 s

Figure 8. Cracked states at the time of t = 4,871 s, t = 4,89 s and t=5,08 s for the B group soil.

The first damage in the soil groups C occurred at 4,411 s around the mid-region of the dam-soil interface where the stress concentrations on the upstream side occurred and the tensile stress reached high values and as the dam crest continued its movement in the flow direction (Figure 9.a). There was no significant change in this crack area until 4,42 s, when the movement of the dam crest continued in the flow direction (Figure 9.b).

At 4,5 s, when the analysis was terminated due to damage and the dam crest moved in the opposite direction to the flow, the existing crack area expanded slightly both in the directions of the slope and the flow (Figure 9.c).

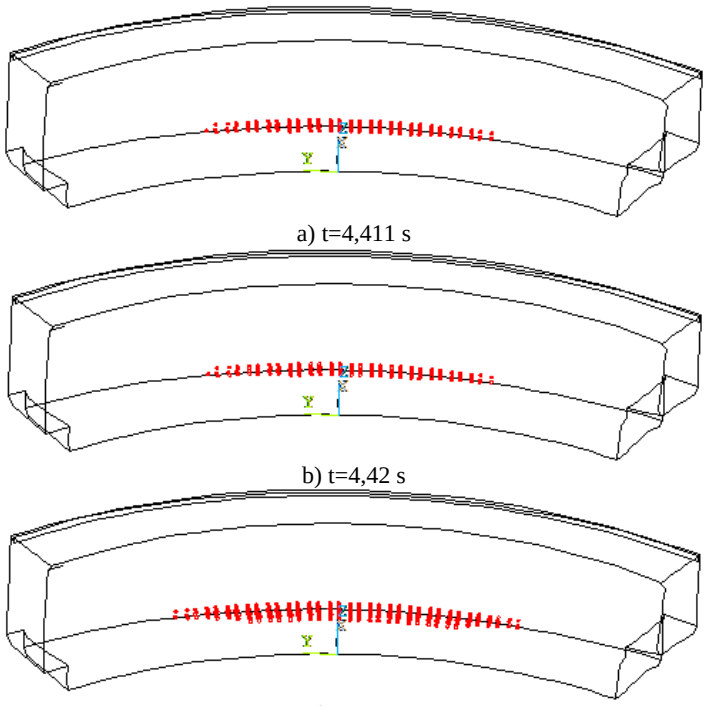

Figure 9. Cracked states at the time of t = 4,411 s, t = 4,42 s and t=4,5 s for the C group soil

The first damage to the dam for the soil group D occurred at 3,971 s at a small area in the downstream region where the tensile stress concentrations occurred and the tensile stress values reached high values as the dam crest continued to move in the opposite direction to the flow (Figure 10.a). There was a slight expansion in the same crack area at 4,0 s, when the movement of the dam crest was in the opposite direction to the flow (Figure 10.b). At 5,071 s, when the dam crest continued to move in the same direction, there was a further enlargement in the same fracture area, while an additional fracture zone appeared at the downstream side where the dam-soil interface intersected the left shoulder (Figure 10.c). At 5,081 s, an additional expansion was observed in the two fracture regions during the movement of the dam crest in the same direction, and an additional fracture region appeared at the junction of the crest and the right slope in the downstream side (Figure 10.d). The fracture progression continued in the three crack zones at 5,1 s, when the dam crest continued to move in opposite direction to the flow.

On the downstream side, the fractures at the point where the crest intersected with the right shoulder spread downwards parallel from the crest to the right shoulder (Figure 10.e). At 5,18 s, when the analysis was terminated due to damage and the dam crest moved in the opposite direction to the flow, but the crest displacement was almost zero, the damage in dam-soil interface crack areas, especially the damage in right slope side, increased significantly. Downward fracture propagation parallel to the slope where the crest intersected the right slope almost covered the whole right slope (Figure 10.f).

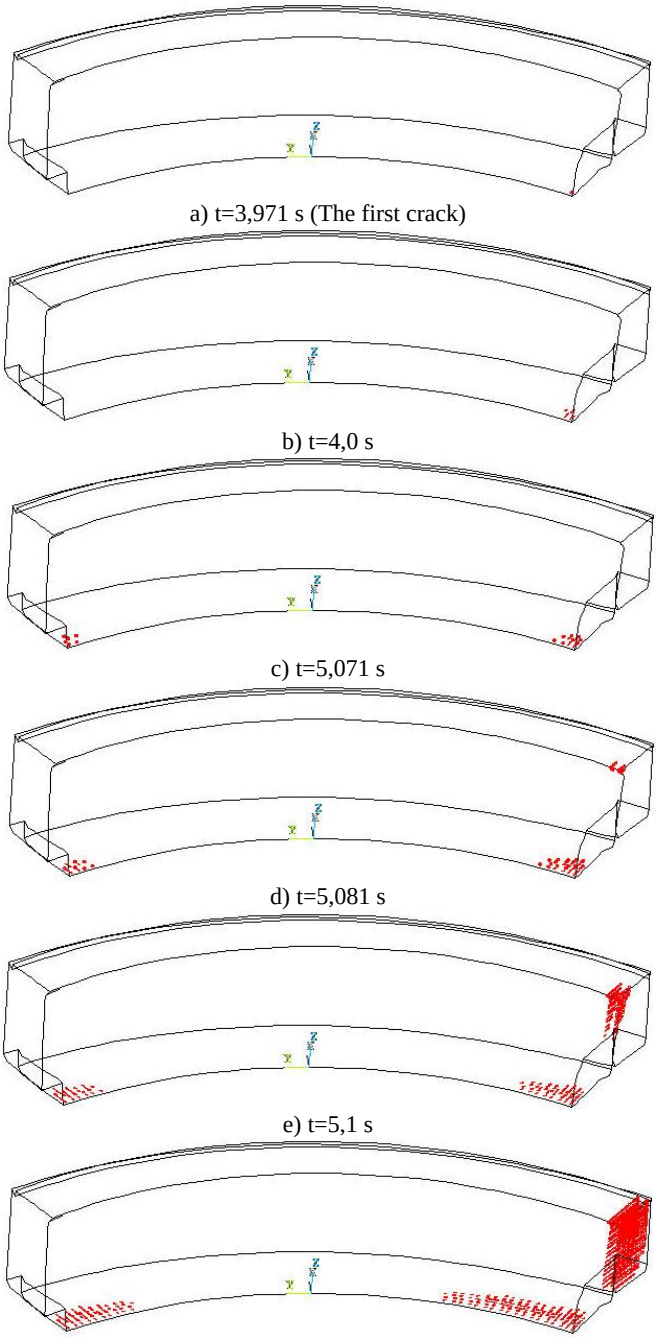

a) t=3,971 s (The first crack)

b) t=4,0 s

c) t=5,071 s

d) t=5,081 s

e) t=5,1 s

f) t=5,18 s

Figure 10. Cracked states at the time of t = 3,971 s, t=4,0 s, t=5,071 s, t=5,081 s, t=5,1 s and t=5,18 s for the D group soil

As a result, there were significant absolute value increases in the maximum and minimum displacements of the dam crest in the flow direction as the soil group changed from A to D (as the soil softened). No damage occurred in the dam due to the seismic effect in the soil group A. In B and C soil groups, the first damage occurred in the mid-region of the dam-soil interface on the upstream side and expanded in the same region over time. However, the ultimate damage for the B soil group was greater than the C soil group. For the D soil group, unlike B and C soil groups, the first damage occurred in the area where the dam-soil interface and the right slope intersected in the downstream side. In the following time steps, the damage was observed in two different areas on the downstream side, where the dam-soil interface intersected with the left slope and where the crest intersected with the right slope. The damage in the abovementioned three areas expanded further over time, and especially in the area where the crest intersected with the right slope, a large damage occurred downstream parallel to the slope. Thus, it could be said that the soil flexibility significantly affected the seismic behavior of the dam.

5. CONCLUSION

In this study, the effect of soil flexibility on the nonlinear seismic behavior of the historical Sultan Mahmut Dam was examined. The smeared crack model that takes strain softening into account was used. It was accepted that reservoir and soil domains demonstrated linear behavior. For D2 earthquake level, artificial earthquake acceleration records were generated in accordance with design spectrum for A, B, C and D soil groups. These acceleration records influenced the dam-soil-reservoir system in the flow direction. As the soil group changed from A to D (as the soil softened), significant absolute value increases were observed in the maximum and minimum displacements of the dam crest in the flow direction. For the soil group A, no damage was observed in the dam. In B and C soil groups, the first damage occurred in the mid-region of the dam-soil interface in the upstream side and further expanded slightly in the same region in time. However, the final damage for soil group B was greater than the soil group C. For the soil group D, the first damage occurred in the downstream side of the intersection of the dam-soil interface and the right slope. The damage was observed in two different areas on the downstream side, where the dam-soil interface intersected with the left slope and where the crest intersected with the right slope in the following time steps. The damage in the abovementioned three areas expanded further over time, and especially in the area where the crest intersected with the right slope, a large damage occurred downstream parallel to the slope. Thus, it could be said that the soil flexibility significantly affected the seismic behaviour of the dam.

REFERENCES

[1] Modena, C., Valluzzi, M.R., Tongini, F.R., and Binda L., "Design choices and intervention techniques for repairing and strengthening of the Monza Cathedral Bell-Tower", Constr. Build. Mater., 16, 385-395, 2002.

[2] Betti, M., and Vignoli, A., "Modelling and analysis of a Romanesque Church under earthquake loading: Assessment of seismic resistance", Engineering Structures, 30, 352–367, 2008.

[3] Riva, P., Perotti, F., Guidoboni, E., and Boschi, E., "Seismic analysis of the Asinelli Tower and earthquakes in Bologna", Soil Dynamics and Earthquake Engineering, 17(7-8), 525-550, 1998.

[4] Fanning, P.J., and Boothby, T.E., "Three-dimensional modeling and full-scale testing of stone arch bridges", Computers and Structures, 79, 2645-2662, 2001.

[5] Bernardeschi, K., Padovani, C., and Pasquinelli, G., "Numerical modeling of the structural behavior of Buti's Bell Tower", J. Cultural Heritage, 5, 371-378, 2004.

[6] Bayraktar, A., Şahin, A., Özcan, D., and Yıldırım, F., "Numerical damage assessment of Hagia Sophia Bell Tower by nonlinear FE modelling", Applied Mathematical Modelling, 34, 92-121, 2010.

[7] Mridha, S., and Maity, D., "Experimental investigation on nonlinear dynamic response of concrete gravity dam-reservoir system", Engineering Structures, 80, 289-297, 2014.

[8] Soumya, Pandey, A.D., Das, R., Mahesh, M.J., Anvesh, S., and Saini, P., "Structural analysis of a historical dam" Procedia Engineering, 144, 140-147, 2016.

[9] Sayın, E., "Nonlinear seismic response of a masonry arch bridge", Earthq. Struct., 10(2), 483–494, 2016.

[10] Sayın, E., Karaton, M., and Calayır, Y., "Nonlinear seismic analyses of historical Topuzlu Dam under different seismic loads", Gradevinar, 68(11), 919-925, 2016.

[11] Karaton, M., Aksoy, H.S., Sayın, E., and Calayır, Y., "Nonlinear seismic performance of a 12th century historical masonry bridge under different earthquake levels", Engineering Failure Analysis, 79, 408–421, 2017.

[12] Zacchei, E., Molina, J.L., and Brasil, R., "Seismic hazard and structural analysis of the concrete arch dam (rules dam on Guadalfeo river)", Procedia Engineering, 199, 1332–1337, 2017.

[13] Yazdani, Y., and Alembagheri, M., "Nonlinear seismic response of a gravity dam under near-fault ground motions and equivalent pulses", Soil Dynamics and Earthquake Engineering, 92, 621–632, 2017.

[14] Wang, G., Wang, Y., Lu, W., Yu, M., and Wang, C., "Deterministic 3D seismic damage analysis of Guandi concrete gravity dam: A case study", Engineering Structures, 148, 263–276, 2017.

[15] Chung, J., and Hulbert, G.M., "A Time integration algorithm for structural dynamics with improved numerical dissipation: the generalized-α method", Journal of Applied Mechanics, 60, 371-375, 1993.

[16] Çeçen, K., "Taksim ve Hamidiye Suları", İSKİ Yayınları, İstanbul, 1992 (in Turkish).

[17] Lourenço, P.B., "Computational strategies for masonry structures", Ph.D. Thesis, Delft Technical University of Technology, The Netherlands, 1996.

[18] Manfredi, C., and Ramasco, R., "The use of damage functionals in earthquake engineering: A comparison between different methods", Earthquake Engineering and Structural Dynamics, 22(10), 855-868, 1993.

[19] Rajgelj, S., Amadio, C., and Nappi, A., "An internal variable approach applied to the dynamic analysis of elastic-plastic structural systems", Earthquake Engineering and Structural Dynamics, 22(10), 885-903, 1993.

[20] William, K.J., and Warnke, E.P., "Constitutive model for the triaxial behaviour of concrete", Proceeding of the International Association for Bridge and Structural Engineering, ISMES, Bergamo, Italy, 1975, 19.

[21] Zeinkiewicz, O.C., and Taylor, R.L., "Finite Element Method", vol. 2, McGraw-Hill, 1991, 84-95.

[22] Cavicchi, A., and Gambarotta, C., "Collapse analysis of masonry bridges taking into account arch fill interaction", Engineering Structures, 27, 605-615, 2005.

[23] ANSYS, (2015), Swanson Analysis System, USA.

[24] DLH-2007, "Earthquake technical regulations relating to coastal, harbor, railway and airport constructions", Ministry of Transportation, Ankara, Turkey, 2007, 6-9 (in Turkish).